Bulk, surface properties and water uptake mechanisms of salt/acid amorphous composite systems

Stefano Bianco, Frederic Tewes, Lidia Tajber, Vincent Caron, Owen I. Corrigan, Anne Marie Healy

*Graphical Abstract (for review)

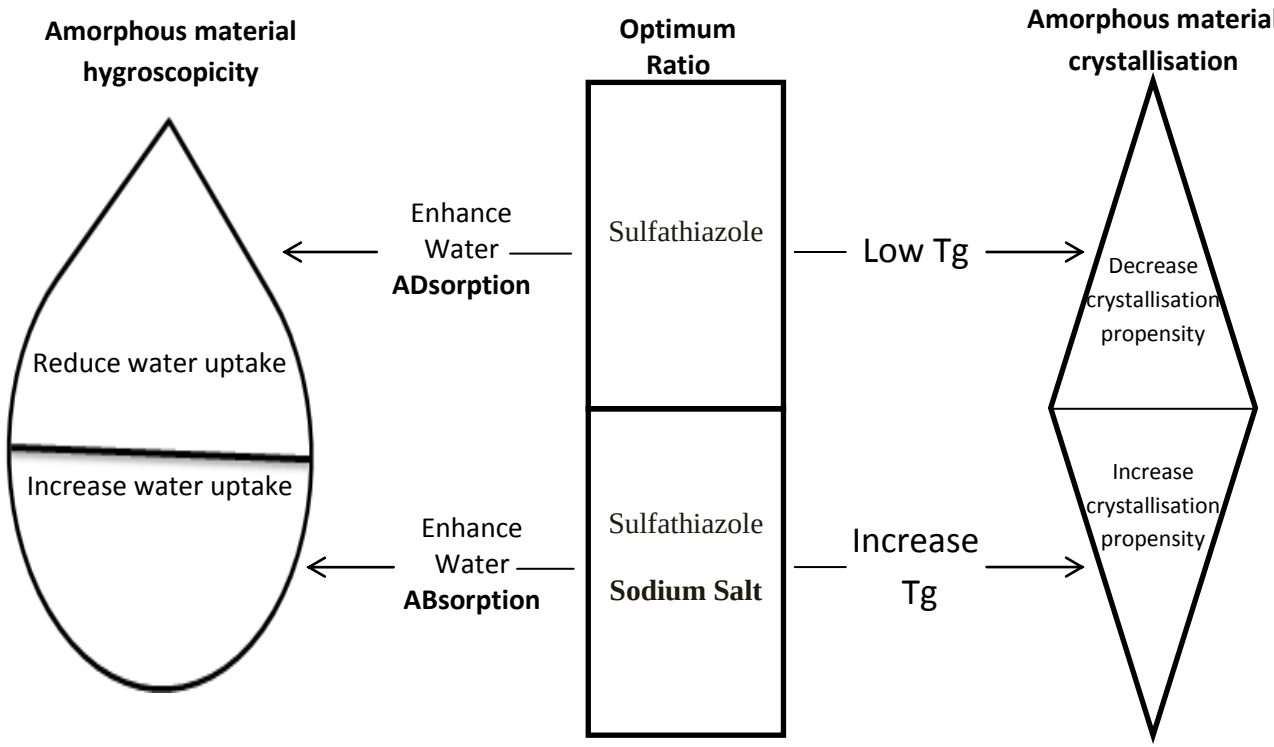

Bulk, surface properties and water uptake mechanisms of salt/acid amorphous composite systems

Stefano Bianco[1], Frederic Tewes[1,2], Lidia Tajber[1], Vincent Caron[1], Owen I. Corrigan[1] and Anne Marie Healy[1,*]

1- School of Pharmacy and Pharmaceutical Sciences, Trinity College Dublin, College Green, Dublin 2, Ireland.

2- INSERM U 1070, Pôle Biologie-Santé, Faculté de Médecine & Pharmacie, Université de Poitiers, 1 rue Georges Bonnet, 86000 Poitiers, France

* To whom correspondence should be sent. Ph.: 00 353 1896 1444, e-mail: healyam@tcd.ie

Abstract

Developing amorphous pharmaceuticals can be desirable due to advantageous biopharmaceutical properties. Low glass transition temperature (Tg) amorphous drugs can be protected from crystallisation by mixing with high Tg excipients, such as polymers, or with salt forms. However, both polymers and salts can enhance the water uptake. The aim of this study was to formulate physico-chemically stable amorphous materials, by co-processing different proportions of sulfathiazole and its sodium salt to produce an optimum ratio, characterised by the best physical stability and lowest hygroscopicity. Both sulfathiazole and salt amorphised upon spray drying. At room temperature, sulfathiazole crystallised within 1 hour at <5% relative humidity while the salt deliquesced when exposed to ambient humidity conditions. In the case of composite systems, FTIR spectroscopy, thermal and surface analysis suggested interactions with an acid:salt stoichiometry of 1:2. Increasing proportions of salt raised the Tg, enhancing the storage stability, however this was opposed by an enhanced hygroscopicity. The water uptake mechanism within the different amorphous systems, analysed by fitting the water sorption isotherms with the Young and Nelson equation, was dependent on the ratio employed, with the salt and the acid facilitating absorption and adsorption, respectively. Tuning the properties of amorphous salt/acid composites by optimising the ratio appears potentially promising to improve the physical stability of amorphous formulations.

1. Introduction

The requirement to improve the bioavailability of poorly soluble active pharmaceutical ingredients (API) has resulted in a growing use of processes such as milling and spray drying, which reduce particle dimensions and increase specific surface area. It is well established that partial or full amorphisation of an API can occur as a result of these processes and that changes in the solid state nature can alter the physicochemical and biopharmaceutical properties (Caron et al., 2011; Tajber et al., 2005; Yu, 2001). Amorphous materials are structurally disorganised and have different bulk and surface properties compared to the corresponding crystalline materials. They typically display higher surface free energy (Newell et al., 2001b), higher hygroscopicity (Newman et al., 2008), greater solubility and a higher dissolution rate (Tajber et al., 2005). Although these properties are relevant from a pharmaceutical development perspective, the full exploitation of amorphous drugs and formulations cannot always be achieved, mainly due to low physical and chemical stability (Caron et al., 2011; Yu, 2001). Therefore a thorough understanding of the properties of the amorphous state is required to develop new strategies to physico-chemically stabilise amorphous compounds.

Previously, we studied several physicochemical properties of sulfathiazole (ST) and sulfathiazole sodium (STNa), which solidify into unstable amorphous materials on spray drying (Bianco et al., 2012). The acid rapidly crystallised regardless of the relative humidity (RH) conditions. The crystallisation of amorphous solids can be promoted by heat and therefore these materials usually require storage at temperatures well below their glass transition temperature (Tg) (Caron et al., 2011; Hancock et al., 1995; Yu, 2001). Considerable effort has been made to address this problem, either by co-processing heat labile amorphous drugs with high Tg excipients (Caron et al., 2011) or by using amorphous salt forms of these compounds (Tong et al., 2002; Tong and

Zografi, 1999). In many cases a shift of the Tg to higher temperature has been achieved, which is potentially a good strategy to stabilise amorphous formulations. However this is not always sufficient and other influential factors affecting stability must also be considered. For instance, amorphous STNa was characterised by a 60°C increase in Tg compared to ST and was physically stable when stored under desiccated conditions. Nevertheless, it deliquesced when exposed to ambient RH conditions (Bianco et al., 2012).

Deliquescence together with adsorption, capillary condensation, hydrate formation and absorption, is one of the known mechanisms of solid-water interactions (Airaksinen et al., 2005; Hiatt et al., 2011). It is a first order phase transition that happens when a water soluble solid generates a saturated solution by dissolving into the water sorbed from the environment at a specific relative humidity (RH_0) characteristic for that solid. Due to high void space and enlarged free volume relative to the crystalline state, amorphous substances absorb water below RH_0 and undergo deliquescence at a lower RH compared to their crystalline counterparts (Mikhailov et al., 2009). The amount of water absorbed into amorphous materials is proportional to the volume/weight of the amorphous solid and high absorption and retention of water can enhance chemical reactions which may lead to product degradation (Hancock and Shamblin, 1998). Furthermore, sorbed water as well as heat can promote the crystallisation of amorphous materials (Baird and Taylor, 2012; Burnett et al., 2006).

Therefore strategies to stabilise amorphous materials should aim at both increasing the Tg and protecting the amorphous system from water uptake. Co-formulation of a deliquescent salt form (sodium ascorbate) with excipients (maltodextrins) was seen to reduce the moisture sorption and enhance the physical stability of this salt (Hiatt et al., 2011). It was also observed that the

79 production of molecular dispersions of indomethacin and indomethacin sodium via evaporation
80 under vacuum influenced the physicochemical characteristics of each species (Tong and Zografi,
81 2001).

82 The aim of the current research was to improve the physical stability of amorphous ST/STNa
83 mix in terms of crystallisation and deliquescence by adjusting the salt/acid ratio in the composite
84 systems.

85

2. Materials and Methods

2.1 Materials

Sulfathiazole (ST) form III and sulfathiazole sodium (STNa) anhydrous were purchased from Sigma Ireland. Ethanol (99.5% v/v) was purchased from Corcoran Chemicals (Ireland) and deionised water produced by a Millipore Elix Advantage water purification system.

2.2 Spray drying

Spray dried powders were obtained using a Buchi B-290 Mini Spray dryer (Buchi Laboratoriums-Technik AG, Flawil, Switzerland) operating in an open cycle mode configuration using air as the drying gas. 0.5% w/v feed solutions were prepared by dissolving the APIs (Table 1) in a mixture of ethanol and deionised water at a v/v ratio of 9:1, as previously described (Bianco et al., 2012). Spray drying of ST and ST-STNa systems was performed using the following parameters: gas flow of 40 mm (473 L/hr); aspirator rate of 100% and feed flow rate of 30% (8 ml/min). The inlet temperature for the mixtures was adapted to the amount of salt employed in the system ranging from 85 to 90°C and reported in table 1. The salt alone was instead spray dried with an inlet of 160°C so as to produce a dry powder (Bianco et al., 2012). Samples were transferred to Amebis humidity devices (Amebis Ltd., Ireland) at <5% RH (Bianco et al., 2012) and stored in a cold room at 5±1°C immediately after spray drying.

Table 1: Spray drying parameters for ST: STNa systems. (An inlet temperature higher than 85°C for ST 9:1 resulted in partially crystalline materials. For the other systems an inlet temperature lower than 90°C resulted in wet powders).

ST: STNa Weight ratio (w/w)	Code	Inlet (°C)
9:1	ST 9:1	85
8:2	ST 8:2	90
3:1	ST 3:1	90
3:2	ST 6:4	90
1:1	ST 1:1	90
4:6	ST 4:6	90
1:3	ST 1:3	90
15:85	ST 15:85	90

2.3 Thermal analysis

Differential scanning calorimetry (DSC) runs were conducted on a Mettler Toledo DSC 821[e] (Mettler Toledo Ltd., Greifensee, Switzerland) using nitrogen as a purge gas. Samples (3-7 mg) were placed in closed aluminium pans with three vent holes and were heated at a scanning rate of 10 °C/min from 25°C to 280°C. The thermograms ($n \geq 2$) were analysed by Mettler Toledo STAR[e] software.

Modulated temperature DSC (MTDSC) scans were recorded on a QA-200 TA instruments (TA instruments, United Kingdom) calorimeter using nitrogen as a purge gas. Weighed samples (1.5-3.5 mg, $n \geq 2$) were sealed in closed aluminium pans with one pin-hole. The method selected was similar to that previously reported by (Caron et al., 2011). A scanning rate of 1°C/min, amplitude of modulation of 1°C and modulation frequency of 1/60 Hz were employed for all the experiments. The temperature range was from 5°C to 200°C.

2.4 Powder X-ray diffraction (XRD)

X-ray powder diffraction measurements were conducted using a low background silicon sample holder and a Rigaku Miniflex II desktop X-ray diffractometer (Rigaku, Tokio, Japan) as previously described (Caron et al., 2011; Tewes et al., 2013). The samples ($n \geq 2$) were scanned over a range of 5-40° in 2θ scale using a step size of 0.05°/s. The X-ray source was a Cu Kα radiation (λ =1.542 Å) and the diffractometer was operated with a voltage of 30 kV and a current of 15 mA.

2.5 Attenuated total reflection Fourier transform infra-red spectroscopy (ATR-FTIR)

Infrared spectra were produced using a PerkinElmer Spectrum one FT-IR Spectrometer and evaluated using Spectrum v5.0.1 software as previously described (Grossjohann et al., 2012; Tewes et al., 2011). An average of 6 scans with a resolution of 4 cm^{-1} over a wavenumber region of 4000-650 cm^{-1} was used for each sample. All spectra were baseline corrected. The spectrum of pure STNa was subtracted from the mixture spectra, considering their molar ratio.

2.6 Scanning electron microscopy (SEM)

SEM micrographs of samples were taken using a Tescan Mira XMU (Brno, Czech Republic) SEM. The dry powder samples were fixed on aluminium stubs with double-sided adhesive tape and a 10 nm-thick gold film was sputter coated on the samples before visualisation. Primary electrons were accelerated under a voltage of 5 kV. Images were formed from the collection of secondary electrons.

2.7 Water sorption analysis

Water sorption behaviour of samples was determined using a DVS Advantage 1 apparatus (DVS Surface Measurement Systems, London, UK), as previously described (Tewes et al., 2010). Samples placed in a microbalance were exposed to three cycles of RH (0–90–0 %) at 25°C, with the following steps: 3, 6, 10 and then every 10% RH (n=3). Water sorption isotherms were calculated using the equilibrated mass (dm/dt ≤ 0.002 mg/min for 10 min) recorded at the end of each stage and expressed as a percentage of the dry sample mass. The Young–Nelson equations were used to fit experimental equilibrium sorption and desorption data of the isotherms (Tewes et al., 2010):

$$M_s = A(\beta + \theta) + B\theta\, RH \quad (1)$$

$$M_d = A(\beta + \theta) + B\theta\, RH_{\max} \quad (2)$$

where M_s and M_d are, respectively, the mass percentage of water contents of the system at equilibrium for each %RH during sorption and desorption. A and B are constants characteristic of each system and defined by the following equations:

$$A = \delta w \mathrm{Vol_M}/(\mathrm{W}m) \quad (3)$$

$$B = \delta w \mathrm{Vol_A}/(\mathrm{W}m) \quad (4)$$

where δw is the density of the water, $\mathrm{Vol_M}$ and $\mathrm{Vol_A}$ are respectively the adsorbed and absorbed water volumes and $\mathrm{W}m$ is the weight of the dry material.

In this model, θ is the fraction of the surface covered by at least one layer of water molecules. It is defined as follows, with E a constant depending on the material.

$$\theta = RH/(RH + E(1 - RH)) \quad (5)$$

β is defined by the following equation:

$$\beta = -E \times RH/(E - RH \times (E-1)) + E^2/(E-1) \times \ln\left[E - RH(E-1)/E\right] - (E+1) \times \ln(1-RH) \quad (6)$$

Thus, $A\theta$ is the mass of water in a complete adsorbed monolayer expressed as a percentage of the dry mass of the sample. $A(\beta+\theta)$ is the total amount of adsorbed water, and $A\beta$ is the mass of water which is adsorbed beyond the mass of the monolayer (i.e., in multilayer or cluster adsorption). B is the mass of absorbed water at 100% of RH, and, hence, $B\theta$RH is the mass of absorbed water when the water coverage is θ for a given %RH. According to the model characteristics, from the estimated values of A, B, and E, the corresponding profiles of water adsorbed in monolayer ($A\theta$), multilayer ($A\beta$) and absorbed ($B\theta RH$) were obtained.

2.8 Surface free energy measurement

Surface free energy measurements were carried out using inverse gas chromatography (iGC) (SMS Ltd., London, UK), as described previously (Tewes *et al*., 2011). Powders were packed into silanised glass columns (300mm x 3mm). The columns were pre-treated for 1 h at 30°C and 0% RH to remove any physisorbed molecules. Then, 250 µL of the elution mixture (probe vapour and helium) was injected into the carrier gas (helium) flow. All injections of probe vapours were performed at 0.03% v/v of the saturated probe vapour. A flame ionization detector was used to monitor the elution of probe vapours. Measurements were performed at 0, 10 and 20% of RH and 30°C, (n = 2). In acid-base theory, the total surface free energy of a solid (γ_s^T) has 2 main components: a dispersive contribution (γ_s^d) and a specific or acid-base contribution (γ_s^{AB}), which are independent and additive, according to Eq. (7).

$$\gamma_s^T = \gamma_s^d + \gamma_s^{AB} \quad (7)$$

In order to calculate γ_s^d of the powders, alkane probes with a known dispersive contribution (γ_p^d) and a nil specific contribution (γ_p^{AB}) were used. Methane was used as inert reference to determine the dead volume of the system. At this low % of saturation (0.03% v/v), iGC was used in infinite dilution conditions and γ_s^d was calculated using the method developed by Schultz *et al.* (Schultz et al., 1987). γ_s^{AB} was obtained indirectly via the measurement of the specific free energy of adsoption (ΔG^{SP}) of 2 monopolar probes and by using the acid-base theories developed by Van Oss *et al.* (vOCG) (Van Oss et al., 1988). In the vOCG theories, γ_s^{AB} is subdivided into two non-additive parameters γ_s^+ and γ_s^- related according to Eq. (8), representing the electron acceptor (acid) and donor (base) properties, respectively.

$$\gamma_s^{AB} = 2\sqrt{\gamma_S^+ \gamma_S^-} \qquad (8)$$

By using ethyl acetate (γ_p^- = 475.67, γ_p^+ = 0 mJ/m^2, at 30^{o}C) as the base probe and dichloromethane (γ_p^- = 0, γ_p^+ = 124.58 mJ/m^2, at 30^{o}C) as the acid probe with the acid and base component values calculated based on the Della Volpe and Siboni scale (Della Volpe and Siboni, 1997), γ_s^+ and γ_s^- of the surface of the powders were calculated. Polarity index (γ_S^{AB}/γ_S^d) was then calculated.

Additionally the spreading coefficient (S_{SL}) was calculated using the dispersive contribution (γ_s^d) and the acid-base contribution (γ_s^+ and γ_s^-) of the total surface free energy of the solid and of the liquid (water) by the following equation.

$$S_{SL} = 2.\sqrt{\gamma_S^d \gamma_L^d} + 2.\sqrt{\gamma_S^+ \gamma_L^-} + 2.\sqrt{\gamma_S^- \gamma_L^+} - 4.\sqrt{\gamma_L^+ \gamma_L^-} - 2\gamma_L^d \qquad (9)$$

Where γ_L^d, γ_L^+ and γ_L^- are respectively the dispersive contribution (γ_L^d) and the acid-base contribution (γ_L^+ and γ_L^-) of the total surface free energy of the of the liquid (water) (Zdziennicka and Jańczuk, 2010).

2.9 Density measurements

The density of spray dried ST and STNa was measured by an Accupyc 1330 Pycnometer (Micromeritics ®) using helium (99.995% purity) to determine the volume of the sample. Samples were dried prior to measurement for 24 h in a Gallenkamp vacuum oven operating at 600 mbar and 25°C.

2.10 Statistical analysis

Data were statistically evaluated by a two-way analysis of variance (ANOVA) test with Bonferroni test as post-hoc test. Significance level was $\alpha < 0.05$.

3. Results and discussion

3.1 PXRD, DSC and FTIR analysis of spray dried systems

Previous experiments showed that ST and STNa solidified into amorphous materials on spray drying. However, both spray dried substances were physically unstable. Amorphous ST started to crystallise to polymorph I ~30 minutes after the end of the spray drying process regardless of the temperature and RH of storage. In contrast, spray dried STNa remained amorphous when stored for over a year in desiccated conditions at 5±1°C. Nevertheless, amorphous STNa rapidly deliquesced at ambient conditions (18-22°C and 40-80% RH) (Bianco et al., 2012).

All ST: STNa spray dried composites presented a diffuse halo pattern, characteristic of XRD amorphous materials (Fig. 1).

Figure 1: PXRD patterns of: (a) unprocessed ST (form III); b) spray dried ST; c) spray dried ST 9:1; d) spray dried ST 3:1; e) spray dried ST 1:1; f) spray dried ST 1:3; g) spray dried STNa; h) unprocessed STNa.

The ST: STNa ratio employed and the storage conditions influenced the physical stability of the processed powders. For example, in desiccated conditions at 5°C, by using just 10% w/w of the salt form, the resulting composite remained amorphous for ~2 months as observed by PXRD. Higher amounts of salt in the composites increased the stability by up to 5 months for ST 3:1 and by six months for ST 1:1 and ST 1:3.

SEM images showed that ST: STNa composite samples were homogeneous and consisted of spherical smooth particles with surface indentations for systems comprising up to 50% w/w STNa (Fig. 2a-b-c). In contrast, no discrete particles were detected by SEM for a higher STNa content. Both ST 1:3 (Fig. 2d) and STNa deliquesced, indicating a higher affinity of these two samples for water compared to the other systems.

Figure 2: SEM micrographs of: a) spray dried ST 9:1; b) spray dried ST 3:1; c) spray dried ST1:1; d) spray dried ST1:3.

Previously reported thermal analysis of pure spray dried ST showed an exotherm of crystallization at 79±0.5°C followed by an endotherm of melting at 201±0.5°C while the amorphous salt crystallised above 160°C and melted at 268±0.2°C (Bianco et al., 2012). Spray dried ST 9:1, ST 8:2, ST 3:1 and ST 15:85 (Fig. 3) presented one endothermic event of melting. These composites also showed one exotherm of crystallisation with onset ranging between those of the pure materials. In contrast ST 6:4, ST 1:1, ST 4:6 and ST 1:3 did not show either exothermic or melting peaks on the thermograms. The inhibition of crystallisation upon heating (at 1 or 10°C/min) for these mixtures could be due to the development of molecular interactions between ST: STNa for these specific ST: STNa ratios (Tong and Zografi, 2001).

Figure 3: Heat flow thermograms of: (a) unprocessed ST (form III); b) spray dried ST; c) spray dried ST 9:1; d) spray dried ST 3:1; e) spray dried ST 1:1; f) spray dried ST 1:3; g) spray dried ST 15:85 h) spray dried STNa; i) unprocessed STNa.

The glass transition temperature (Tg) for pure ST and STNa were previously found to be ~59°C and ~120°C, respectively (Bianco et al., 2012). To determine the Tgs of the various composites and distinguish between thermal events which could happen simultaneously upon heating, MTDSC was employed in this work. All reversing heat flow thermograms recorded for the different spray dried systems showed a single Tg, with values between those of the pure materials and increasing with the STNa content. According to several authors (Bosma et al., 1988; Caron et al., 2011; Tong and Zografi, 2001) the detection of a single Tg is indicative of homogeneous amorphous phases (molecular dispersions). Therefore, thermal analysis revealed that the increase of physical stability was due to the introduction of STNa in the mixture which shifted the Tgs to higher temperatures. Measured Tgs and Tg values calculated using the Gordon

Taylor with Simha-Boyer rule (GT – equation 10) (Caron et al., 2011; Tajber et al., 2005) were plotted versus STNa weight fraction (Fig. 4).

$$T_g(mix) = \frac{w_1 T_{g1} + K_{GT} w_2 T_{g2}}{w_1 + K_{GT} w_2} \quad \text{where} \quad K_{GT} = \frac{d_1 T_{g1}}{d_2 T_{g2}} \qquad (10)$$

T_g, w and d are the glass transition temperature in degrees Kelvin, the weight fraction, and density of the subscripts 1 — first component, 2 — second component, respectively.

The true densities for the pure amorphous components of 1.52 g/cm^3 and 1.57 g/cm^3 for ST and STNa respectively, were used in the calculation of theoretical Tg values. The Tgs of the composites were found to deviate positively from the GT predicted values.

Figure 4: **Glass transition temperatures of ST: STNa systems as a function of STNa content (squared markers). The solid line represents the Tg predictions based on the Gordon-Taylor with Simha-Boyer rule equation.**

The Gordon-Taylor equation is widely accepted to predict the Tg of mixtures. The theory affirms that in the ideal mix free volumes are additive and no interaction between the components takes place during mixing (Caron et al., 2011). However, because of the presence of interacting groups in either species, the ST-STNa mixture could, in theory, result in the formation of intermolecular bonds, such as hydrogen or ion-dipole bonding, which should cause an increase in Tg compared to the predicted values. Tong and Zografi also showed positive deviations of Tg from GT predicted values when indomethacin was co-processed with its corresponding sodium salt, suggesting a stronger acid-salt interaction in the amorphous state than that between acid-acid and salt-salt (Tong and Zografi, 2001).

FTIR spectroscopy has been used to investigate molecular interaction between species, included in composites (Caron et al., 2011; Tong and Zografi, 2001). FTIR spectra (1800-1000 cm^{-1}) of spray dried ST, STNa and ST mixed in different proportions with STNa are shown in Fig. 5A.

Figure 5A: FTIR spectrum in the 1800-1000 cm^{-1} range of a) spray dried ST; b) to f) spray dried ST:STNa in the ratios 9:1, 3:1, 1:3, 15:85 and g) FTIR spectrum of spray dried STNa. 5B: Job plot representation

Peak shifts of different magnitudes were recorded, depending on the STNa content, indicative of interactions between the two species (Caron et al., 2011; Tong and Zografi, 2001). For example, in the 3000-3500 cm^{-1} region, the N-H_2 asymmetric stretch peak, which in the spectrum of pure amorphous ST appears at ~3462 cm^{-1}, shifted to lower wavenumbers (data not shown). The shift to lower wavenumbers can be due to weakening of the N-H bond as a result of a stronger involvement in H-bondings (Kaushal et al., 2008; Tang et al., 2002). The simultaneous shift to higher wavenumbers of the C-NH_2 stretching peak (~ 1417 cm^{-1} on the spectrum of ST), confirmed the NH_2 group being increasingly involved in H-bonds (Fig. 5A). In the 1000-1600 cm^{-1} region, shifts to lower wavenumbers were seen for the peaks at 1140 and 1084 cm^{-1}, characteristic of the stretching of both symmetric SO_2 and C-S peaks (Hu et al., 2010). These shifts to lower wavenumbers suggested the SO_2 group as the H-bond acceptor and the development of N–H· · ·O bondings. This type of interaction was previously described to link dimers of ST in polymorph I (Parmar et al., 2007).

The stretching peak shifts of N-H_2 and C-S for the different composites were plotted against the mole fraction of STNa to create a Job plot representation (Fig 5B) in order to determine the stoichiometry of the interaction involving –NH_2 and –SO_2 groups (Likussar and Boltz, 1971). This approach using solid ATR-FTIR was adapted from the study of Osmani *et al.* (Osmani et al., 2008) who generated a Job plot from FTIR C=O band shifting frequency in solution. The STNa molar fraction associated to the maximum of the Job plots, obtained at two wavenumbers, were between 0.6 and 0.7. The ST: STNa molar ratio of 1:2 lies between these two molar fractions. Therefore, from the plot, it appears that one molecule of ST interacted with two

molecules of STNa. This interaction between ST and STNa could be responsible for the lack of thermal events observed on the DSC thermograms obtained for the ST 4:6 and ST 1:3, as the ST: STNa molar ratio of 1:2 falls between these two composites.

3.2 iGC and DVS analysis

iGC was used to more fully investigate the surface of the systems and to assess the possibility of interactions between ST and STNa at the surface of the spray dried particles. Several phenomena of pharmaceutical importance start at the surface, and are critically affected by the surface properties of the substances involved (Buckton and Gill, 2007; Puri et al., 2010). Surface solid-liquid interactions for example, besides affecting processes such as dissolution, can have a deep impact on the stability of the solid, powder flow etc., and are, above all, governed by solid surface free energy (γ_s^T) (Puri et al., 2010). Generally a substance in its amorphous form has a higher γ_s^T than the corresponding crystalline form because of a more random orientation of molecules exposing higher surface energy groups at the particle surface (Brum and Burnett, 2011; Newell et al., 2001a). This γ_s^T differences can have a significant impact on the behaviour of the two solid states (amorphous versus crystalline) upon processing. Differences in the γ_s^T can also be displayed by amorphous samples of the same material obtained with different processing techniques and changes with time due to relaxation can affect the γ_s^T of amorphous material upon storage (Buckton and Gill, 2007).

Figure 6: Total surface free energy for the different weight ratios (ST: STNa) at different %RH. Statistical analysis compares data obtained at the same RH value. System ST 1:3 was taken as reference of comparison for statistical post-hoc analysis. *** P<0.001

As a consequence of the development of interactions between the species included in the processed mixtures, variations of the γ_s^T among the various systems would be expected. STNa

and four different composites were analysed by iGC. The γ_s^T values measured for ST 9:1 and ST 3:1 were not significantly different, and were found to be the highest among the systems studied, at ~53 mJ/m^2 (Fig. 6). The increase in STNa content to the ST 1:3 system decreased significantly the γ_s^T values, down to ~41 mJ/m^2 (P<0.001). Then γ_s^T rose up again for the pure amorphous salt, reaching ~48 mJ/m^2 (Fig. 6). The minimum of γ_s^T obtained for ST 1:3 could be due to a different organisation and/or to the development of interactions between the molecules at the surface of the particles, decreasing the number of chemical groups available to interact with external molecules such as the probe molecules. Moreover, changes in ST: STNa ratio also influenced the polarity of the powder surfaces as shown by the variation in the polarity index (γ_S^{AB}/γ_S^d) in Fig. 7A.

Figure 7: Polarity index (A) and spreading coefficient (B) changes for different weight ratios and %RH. Statistical analysis compares data obtained at the same RH value. System ST 1:3 was taken as reference of comparison for statistical post-hoc analysis *** P<0.001, ** P<0.01, * P < 0.05.

An increase in salt content from ST 9:1 to ST 3:1 raised the polarity index, reaching a value similar to that obtained for pure amorphous STNa. However, a further increase (in salt content) to ST 1:1 and ST 1:3 reduced the surface polarity. The ST: STNa molar ratio 1:2 falls between that of these two systems (i.e. ST 1:1 and ST 1:3), which supports the concept of the development of 1:2 interactions, as previously suggested by FTIR spectroscopy. Therefore, ST-STNa interaction should involve polar bonding, decreasing the amount of polar chemical groups available at the surface to interact with the probe molecules.

Water adsorption is strongly influenced by surface polarity (Bradley et al., 2010). In particular, water vapor molecules can interact with solids through specific hydrogen-bonding with surface

polar groups. Furthermore, when the solid is ionic, water molecules can interact with the components of the solid through ion-dipole interaction. For amorphous solids, the wettability and interaction with water are fundamental aspects to be studied because they can affect both dissolution properties (Puri et al., 2010) and physical stability (Hancock and Zografi, 1994; Puri et al., 2010). Both STNa and ST 1:3 deliquesced when exposed to ambient humidity conditions. Hence, the interaction of the composites with water was investigated by calculating the powder wettability and analysing the water vapor sorption isotherms.

The wettability of a powder by water depends on both the work of adhesion of the water onto the powder surface (W_A) and on the water work of cohesion (W_C). Complete spreading of the water over a powder is possible if the work of adhesion onto the surface is equal to or higher than the work of cohesion among the water molecules (Zdziennicka and Jańczuk, 2010). This difference equals the spreading coefficient (S_{SL}). The S_{SL} of water over the composites, for various %RH, is reported in Fig. 7B. For all systems the S_{SL} was negative, indicating that the spreading of water on the powder surface is not favoured and requires work. For each system, S_{SL} was not affected by a change in the %RH from 0% to 20% but changed depending on the ST: STNa ratio. An increase in salt content from ST 3:1 to ST 1:3 decreased the S_{SL}, indicating a decrease in water affinity for the powder surfaces.

The overlayed DVS 1st sorption isotherm plots of the systems indicated that the whole/entire water uptake increased with the increase of salt content over the entire RH range (Fig. 8). The mass gain recorded at 90% RH was linearly proportional to the STNa content in the composites. The coefficient of determination (r^2) of the linear fit was 0.99. For instance, spray dried STNa mass uptake was 36% w/w of the dry mass and decreased to 3.6% w/w for ST 9:1. As previous

studies on the hygroscopicity of ST after spray drying indicated that the API had a maximum water uptake of only 0.5% at 90% RH (Bianco et al., 2012), the water uptake for the blends is primarily due to the salt.

Figure 8 Water sorption isotherms for spray dried systems with different ST: STNa weight ratios.

The kinetic profiles obtained for systems ST 9:1 (Fig. 9A), ST 3:1 and ST 1:1 showed continuous water uptake versus time before reaching equilibrium for each % RH steps up to 40% RH. For these systems during the 50% RH step an initial mass increase was followed by a decrease in mass. A similar behaviour was also seen for ST 1:3 but the decrease in mass was lower, recorded at a lower RH and in two steps at 30% and 40% RH (Fig. 9B). A decrease in mass versus time with increasing RH for amorphous substances corresponds to the crystallisation of the material (Burnett et al., 2006). The mass loss is attributed to water loss due to the reduced hygroscopicity of a new crystalline phase compared to the amorphous form. Therefore the content of salt in the mixtures influenced the RH at which crystallisation took place by promoting the water uptake which acts as a plasticiser for the mixture.

Figure 9 DVS kinetics (A, B, C) and isotherms (A', B', C') of: A-A') spray dried ST 9:1; B-B') spray dried ST 1:3; C-C') spray dried STNa.

In contrast the kinetics for the pure amorphous STNa did not show any mass loss but a continuous increase in mass with increasing RH (Fig. 9C). Generally, crystalline solids with high solubility such as salts may deliquesce at a RH value lower than 100%, defined as RH_0, which is characteristic of the material. RH_0 of a compound can be determined from the moisture sorption isotherm as a sharp break due to a sudden change in water uptake which takes place at deliquescence (Hiatt et al., 2011). In contrast, when dealing with amorphous solids, deliquescence can be regarded as a non-equilibrium phase transition because water uptake by

amorphous substances proceeds in a gradual way and their transformation from solid to liquid state may involve intermediate semi-solid stages (Mikhailov et al., 2009). It was not possible to determine the RH of deliquescence for amorphous STNa either from the water sorption isotherm (Figure 9C) or the corresponding kinetics (Figure 9C').

Both ST 1:3 and STNa recorded mass uptake of respectively ~4.3% and 7% at the end of the first cycle. The water uptake for amorphous STNa was previously attributed to the crystallisation of the amorphous salt to a sesquihydrate (Bianco et al., 2012). PXRD analysis performed at the end of the water sorption isotherm confirmed that the composites converted to the same sesquihydrate form. Additional mass losses were detected in the kinetics for all composites in the second DVS sorption cycle (Fig. 9). These mass losses were of lower magnitude compared those in the first cycles. These mass losses indicated a not complete (i.e. partial) crystallisation of the amorphous systems at the end of the first sorption cycle. Full crystallisation following exposure to a first full 0-90% RH cycle was not achieved and this may be attributed to water not completely penetrating the bulk of the composites.

If we consider the adsorption process as the only mechanism of interaction between water and the powders, the higher the surface energy, surface polarity and spreading coefficient the greater is the expected water uptake. However, the surface properties measured for the different composites examined did not correlate with the whole water uptake isotherms. The γ_s^T of ST 9:1 and ST 3:1 were greater than those of STNa, ST 1:1 and ST 1:3, respectively. Nonetheless, ST 9:1 and ST 3:1 were characterised by lower water uptake compared to the other systems. Despite having the lowest γ_s^T profile (Fig. 6) among all systems examined, the water uptake of ST 1:3 was the second highest, lower only than STNa. However amorphous materials can either adsorb water, or absorb it in the bulk of the material (Agrawal et al., 2004; Alvarez-Lorenzo et al., 2000;

Bravo-Osuna et al., 2005). Hence, the distribution of water in the different systems was determined by establishing quantitative correlations between equilibrium moisture content and the %RH using the Young and Nelson equations (Agrawal et al., 2004; Alvarez-Lorenzo et al., 2000; Bravo-Osuna et al., 2005; Tewes et al., 2010). Fitting DVS data with the Young–Nelson equations indicated that the water distribution within the different systems was dependent on the ST:STNa ratio. For ST 9:1, adsorption was the main process of water uptake, as can be confirmed by the high value of the *A* parameter, compared to the *B* parameter of the Young-Nelson equations (Fig. 10).

Figure 10: Moisture distribution patterns for 1:3 (A) and 3:1 (B) samples obtained by fitting experimental DVS results with the Young and Nelson equations. Estimated A, B, E Young and Nelson parameters and fit correlation coefficient for all the composites investigated are inserted in the chart (A).

It was found that an increase in STNa content increased the proportion of water absorbed, and water sorption for ST 1:1 and ST 1:3 was mainly by absorption. Fig. 10 shows a comparison of the Young and Nelson distribution patterns of water obtained by fitting DVS results for two systems (A) ST 1:3 and (B) ST 3:1 which are characterised respectively by low and high surface free energy. Most of the water uptake by ST 1:3 was absorbed in the bulk while only a minute amount was adsorbed on the surface. In contrast the water uptake for the higher γ_s^T system ST 3:1 was due to both adsorption and absorption. The higher amount of water adsorbed by ST 3:1 compared to ST 1:3 is consistent with the surface profiles for the two different systems.

Therefore the ratio ST:STNa influenced not only the total hygroscopicity but also the water distribution in the different systems and this may have an important impact on the physical stability of the powders. Several authors have attributed the water uptake by amorphous materials mainly to absorption processes (Alvarez-Lorenzo et al., 2000; Bravo-Osuna et al.,

445 2005; Hancock and Shamblin, 1998). However, according to this study the main water sorption
446 mechanism for the system ST 9:1 was by adsorption, with a minimal amount of water absorbed.

4. Conclusions

This study showed that an extremely unstable amorphous API like sulfathiazole can be protected from crystallisation by co-spray drying it with its corresponding sodium salt form. In particular the addition of just 10% w/w salt was enough to delay the crystallisation of the resulting powder from 1 to 60 days of storage under desiccated conditions. Increasing the proportion of salt in the composite further improved the storage stability; however this was opposed by an increased hygroscopicity. The increased physical stability may be attributed to interactions between the species which cause the shift of Tg to higher temperature. FTIR spectroscopy, iGC and thermal analysis suggested interactions between the species with a stoichiometry of 1 molecule of acid for 2 molecules of salt. For the systems investigated, by analysing the hygroscopic properties it has also emerged that water uptake by an amorphous material could either be mainly by adsorption or by absorption depending on the chemical nature of the material, with the salt facilitating water absorption. Therefore controlling the physico-chemical properties of the composites by varying the ratio of the components can be beneficial to stabilise amorphous formulations. For example among the ST: STNa composites an optimum mixture which provided the best compromise between hygroscopicity and stability was the 1:1 w:w system. In this ratio the amorphous powder was characterised by good physical stability, intermediate water uptake and low surface free energy.

5. Acknowledgement

This paper is based upon works supported by the Science Foundation Ireland under grant no. 07/SRC/B1158, as part of the Solid State Pharmaceutical Cluster (SSPC) and grant no. 07/SRC/B1154, as part of the Irish Drug Delivery Network (IDDN).

6. References

Agrawal, A., M. , Manek, R., V. , Kolling, W., M., Neau, S., H., 2004. Water distribution studies within microcrystalline cellulose and chitosan using differential scanning calorimetry and dynamic vapor sorption analysis. Journal of Pharmaceutical Sciences 93, 1766-1779.

Airaksinen, S., Karjalainen, M., Shevchenko, A., Westermarck, S., Leppänen, E., Rantanen, J., Yliruusi, J., 2005. Role of water in the physical stability of solid dosage formulations. Journal of Pharmaceutical Sciences 94, 2147-2165.

Alvarez-Lorenzo, C., Gómez-Amoza, J.L., Martínez-Pacheco, R., Souto, C., Concheiro, A., 2000. Interactions between hydroxypropylcelluloses and vapour/liquid water. European Journal of Pharmaceutics and Biopharmaceutics 50, 307-318.

Baird, J.A., Taylor, L.S., 2012. Evaluation of amorphous solid dispersion properties using thermal analysis techniques. Advanced Drug Delivery Reviews 64, 396-421.

Bianco, S., Caron, V., Tajber, L., Corrigan, O.I., Nolan, L., Hu, Y., Healy, A.M., 2012. Modification of the Solid-State Nature of Sulfathiazole and Sulfathiazole Sodium by Spray Drying. AAPS PharmSciTech, 1-14.

Bosma, M., Ten Brinke, G., Ellis, T.S., 1988. Polymer-polymer miscibility and enthalpy relaxations. Macromolecules 21, 1465-1470.

Bradley, R.H., Andreu, A., Cassity, K., Osbeck, S., Andrews, R., Meier, M., Johnston, C., 2010. Dependence of water vapour adsorption on the polarity of the graphene surfaces of multi-wall carbon nanotubes. Adsorption Science and Technology 28, 903-912.

Bravo-Osuna, I., Ferrero, C., Jiménez-Castellanos, M.R., 2005. Water sorption-desorption behaviour of methyl methacrylate-starch copolymers: effect of hydrophobic graft and drying method. European Journal of Pharmaceutics and Biopharmaceutics 59, 537-548.

Brum, J., Burnett, D., 2011. Quantification of surface amorphous content using dispersive surface energy: The concept of effective amorphous surface area. AAPS PharmSciTech 12, 887-892.

Buckton, G., Gill, H., 2007. The importance of surface energetics of powders for drug delivery and the establishment of inverse gas chromatography. Advanced Drug Delivery Reviews 59, 1474-1479.

Burnett, D.J., Thielmann, F., Sokoloski, T., Brum, J., 2006. Investigating the moisture-induced crystallization kinetics of spray-dried lactose. International Journal of Pharmaceutics 313, 23-28.

Caron, V., Tajber, L., Corrigan, O.I., Healy, A.M., 2011. A comparison of spray drying and milling in the production of amorphous dispersions of sulfathiazole/polyvinylpyrrolidone and sulfadimidine/ polyvinylpyrrolidone. Molecular Pharmaceutics 8, 532-542.

Della Volpe, C., Siboni, S., 1997. Some reflections on acid-base solid surface free energy theories. Journal of Colloid and Interface Science 195, 121-136.

Grossjohann, C., Eccles, K.S., Maguire, A.R., Lawrence, S.E., Tajber, L., Corrigan, O.I., Healy, A.M., 2012. Characterisation, solubility and intrinsic dissolution behaviour of benzamide: Dibenzyl sulfoxide cocrystal. International Journal of Pharmaceutics 422, 24-32.

Hancock, B.C., Shamblin, S.L., 1998. Water vapour sorption by pharmaceutical sugars. Pharmaceutical Science and Technology Today 1, 345-351.

Hancock, B.C., Shamblin, S.L., Zografi, G., 1995. Molecular mobility of amorphous pharmaceutical solids below their glass transition temperatures. Pharmaceutical Research 12, 799-806.

Hancock, B.C., Zografi, G., 1994. The relationship between the glass transition temperature and the water content of amorphous pharmaceutical solids. Pharmaceutical Research 11, 471-477.

Hiatt, A.N., Taylor, L.S., Mauer, L.J., 2011. Effects of co-formulation of amorphous maltodextrin and deliquescent sodium ascorbate on moisture sorption and stability. International Journal of Food Properties 14, 726-740.

Hu, Y., Erxleben, A., Ryder, A.G., McArdle, P., 2010. Quantitative analysis of sulfathiazole polymorphs in ternary mixtures by attenuated total reflectance infrared, near-infrared and Raman spectroscopy. Journal of Pharmaceutical and Biomedical Analysis 53, 412-420.

Kaushal, A.M., Chakraborti, A.K., Bansal, A.K., 2008. FTIR studies on differential intermolecular association in crystalline and amorphous states of structurally related non-steroidal anti-inflammatory drugs. Molecular Pharmaceutics 5, 937-945.

Likussar, W., Boltz, D.F., 1971. Theory of continuous variations plots and a new method for spectrophotometric determination of extraction and formation constants. Analytical Chemistry 43, 1265-1272.

Mikhailov, E., Vlasenko, S., Martin, S.T., Koop, T., Pöschl, U., 2009. Amorphous and crystalline aerosol particles interacting with water vapor: Conceptual framework and experimental evidence for restructuring, phase transitions and kinetic limitations. Atmospheric Chemistry and Physics 9, 9491-9522.

Newell, H.E., Buckton, G., Butler, D.A., Thielmann, F., Williams, D.R., 2001a. The use of inverse phase gas chromatography to measure the surface energy of crystalline, amorphous, and recently milled lactose. Pharmaceutical Research 18, 662-666.

Newell, H.E., Buckton, G., Butler, D.A., Thielmann, F., Williams, D.R., 2001b. The use of inverse phase gas chromatography to study the change of surface energy of amorphous lactose as a function of relative humidity and the processes of collapse and crystallisation. International Journal of Pharmaceutics 217, 45-56.

536 Newman, A.W., Reutzel-Edens, S.M., Zografi, G., 2008. Characterization of the "hygroscopic" properties
537 of active pharmaceutical ingredients. Journal of Pharmaceutical Sciences 97, 1047-1059.

538 Osmani, Q., Hughes, H., Flavin, K., Hedin-Dahlstrom, J., Allender, C.J., Frisby, J., McLoughlin, P., 2008. The
539 use of FTIR and NMR spectroscopies to study prepolymerisation interactions in nitrogen heterocycles.
540 Analytical and Bioanalytical Chemistry 391, 1229-1236.

541 Parmar, M.M., Khan, O., Seton, L., Ford, J.L., 2007. Polymorph selection with morphology control using
542 solvents. Crystal Growth and Design 7, 1635-1642.

543 Puri, V., Dantuluri, A.K., Kumar, M., Karar, N., Bansal, A.K., 2010. Wettability and surface chemistry of
544 crystalline and amorphous forms of a poorly water soluble drug. European Journal of Pharmaceutical
545 Sciences 40, 84-93.

546 Schultz, J., Lavielle, L., Martin, C., 1987. The role of the interface in carbon-fiber epoxy composites.
547 Journal of Adhesion 23, 45-60.

548 Tajber, L., Corrigan, O.I., Healy, A.M., 2005. Physicochemical evaluation of PVP-thiazide diuretic
549 interactions in co-spray-dried composites - Analysis of glass transition composition relationships.
550 European Journal of Pharmaceutical Sciences 24, 553-563.

551 Tang, X.C., Pikal, M.J., Taylor, L.S., 2002. A spectroscopic investigation of hydrogen bond patterns in
552 crystalline and amorphous phases in dihydropyridine calcium channel blockers. Pharmaceutical
553 Research 19, 477-483.

554 Tewes, F., Gobbo, O.L., Amaro, M.I., Tajber, L., Corrigan, O.I., Ehrhardt, C., Healy, A.M., 2011. Evaluation
555 of HPβCD-PEG microparticles for salmon calcitonin administration via pulmonary delivery. Molecular
556 Pharmaceutics 8, 1887-1898.

557 Tewes, F., Paluch, K.J., Tajber, L., Gulati, K., Kalantri, D., Ehrhardt, C., Healy, A.M., 2013.
558 Steroid/mucokinetic hybrid nanoporous microparticles for pulmonary drug delivery. European Journal of
559 Pharmaceutics and Biopharmaceutics.

560 Tewes, F., Tajber, L., Corrigan, O.I., Ehrhardt, C., Healy, A.M., 2010. Development and characterisation of
561 soluble polymeric particles for pulmonary peptide delivery. European Journal of Pharmaceutical
562 Sciences. 41, 337-352.

563 Tong, P., Taylor, L.S., Zografi, G., 2002. Influence of alkali metal counterions on the glass transition
564 temperature of amorphous indomethacin salts. Pharmaceutical Research 19, 649-654.

565 Tong, P., Zografi, G., 1999. Solid-state characteristics of amorphous sodium indomethacin relative to its
566 free acid. Pharmaceutical Research 16, 1186-1192.

567 Tong, P., Zografi, G., 2001. A study of amorphous molecular dispersions of indomethacin and its sodium
568 salt. Journal of Pharmaceutical Sciences 90, 1991-2004.

569 Van Oss, C.J., Good, R.J., Chaudhury, M.K., 1988. Additive and nonadditive surface tension components
570 and the interpretation of contact angles. Langmuir 4, 884-891.

571 Yu, L., 2001. Amorphous pharmaceutical solids: Preparation, characterization and stabilization.
572 Advanced Drug Delivery Reviews 48, 27-42.

573 Zdziennicka, A., Jańczuk, B., 2010. Behavior of cationic surfactants and short-chain alcohols in mixed
574 surface layers at water-air and polymer-water interfaces with regard to polymer wettability. II.
575 Wettability of polymers. Journal of Colloid and Interface Science 350, 568-576.

Figure(s)

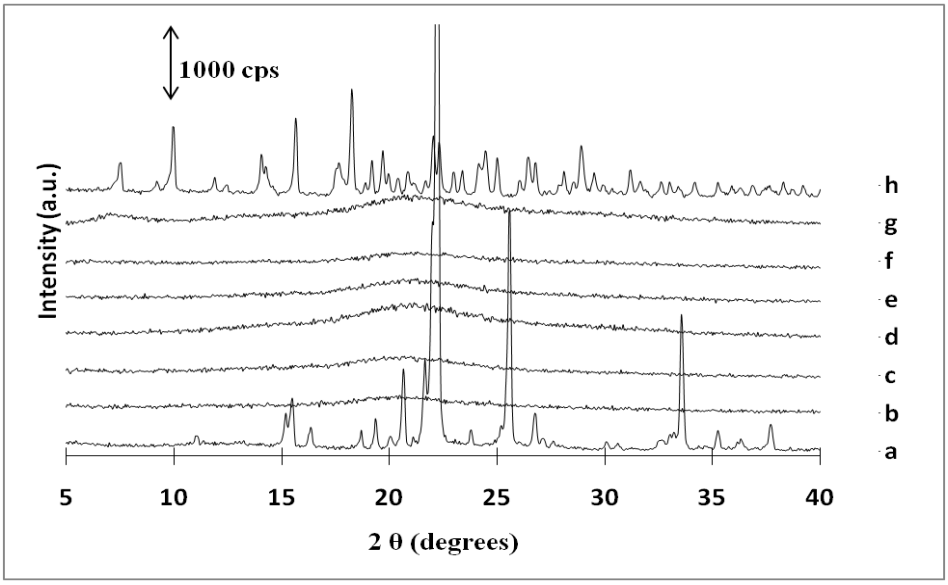

Figure 1: PXRD patterns of: (a) unprocessed ST (form III); b) spray dried ST; c) spray dried ST 9:1; d) spray dried ST 3:1; e) spray dried ST 1:1; f) spray dried ST 1:3; g) spray dried STNa; h) unprocessed STNa.

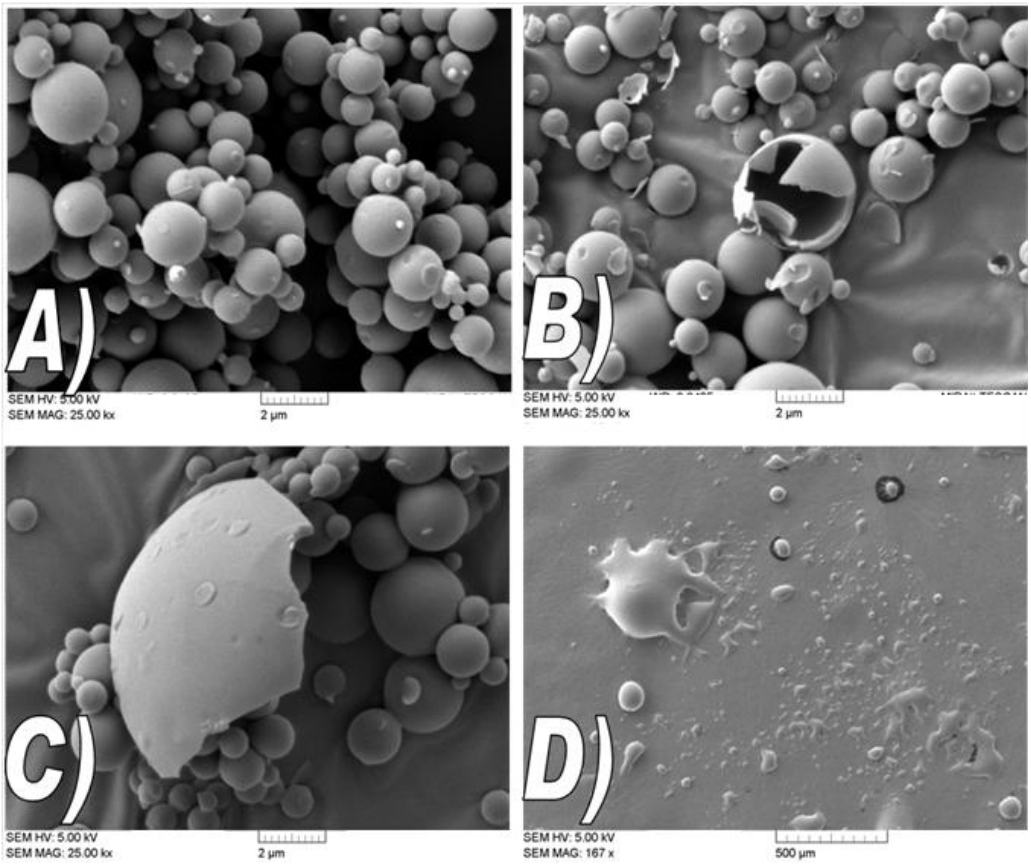

Figure 2: SEM micrographs of: a) spray dried ST 9:1; b) spray dried ST 3:1; c) spray dried ST1:1; d) spray dried ST1:3.

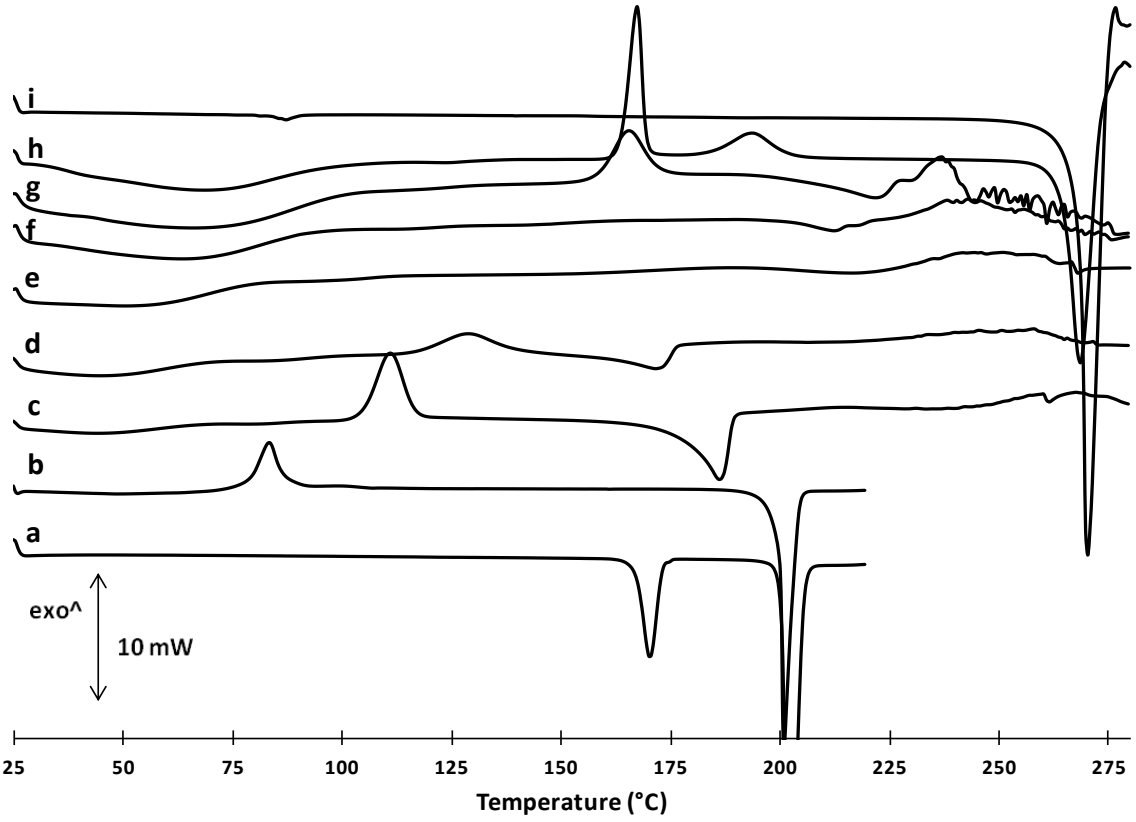

Figure 3 Heat flow thermograms of: (a) unprocessed ST (form III); b) spray dried ST; c) spray dried ST 9:1; d) spray dried ST 3:1; e) spray dried ST 1:1; f) spray dried ST 1:3; g) spray dried ST 15:85 h) spray dried STNa; i) unprocessed STNa.

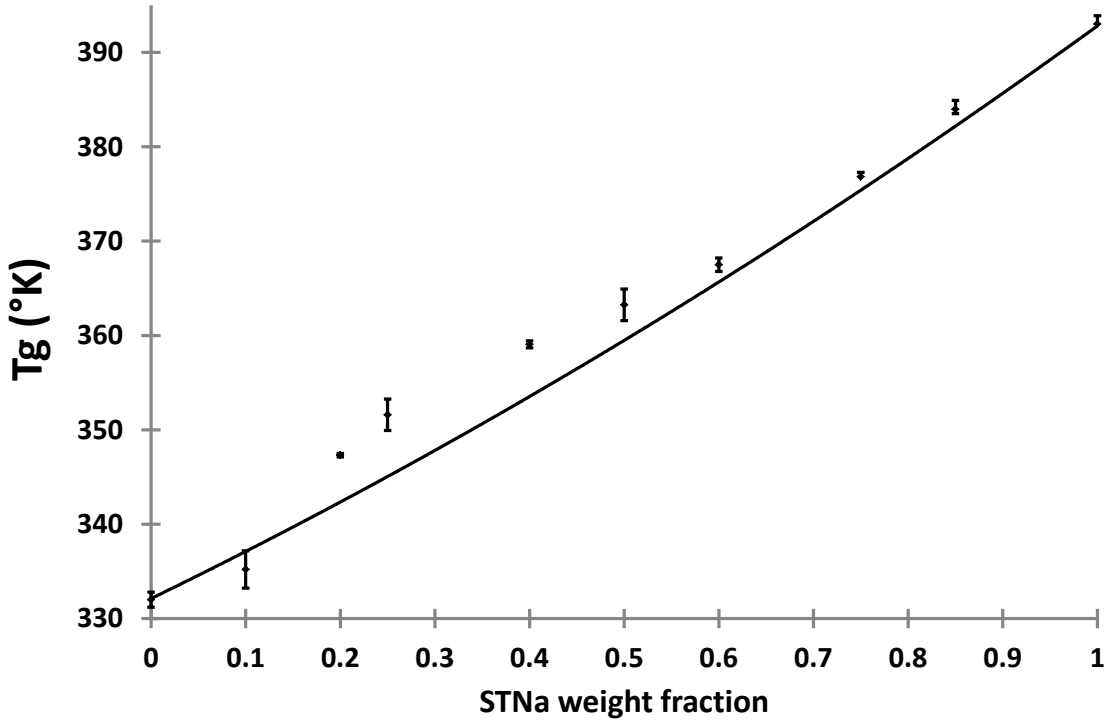

Figure 4: **Glass transition temperatures of ST:STNa systems as a function of STNa content (squared markers). The solid line represents the Tg predictions based on the Gordon-Taylor with Simha-Boyer rule equation.**

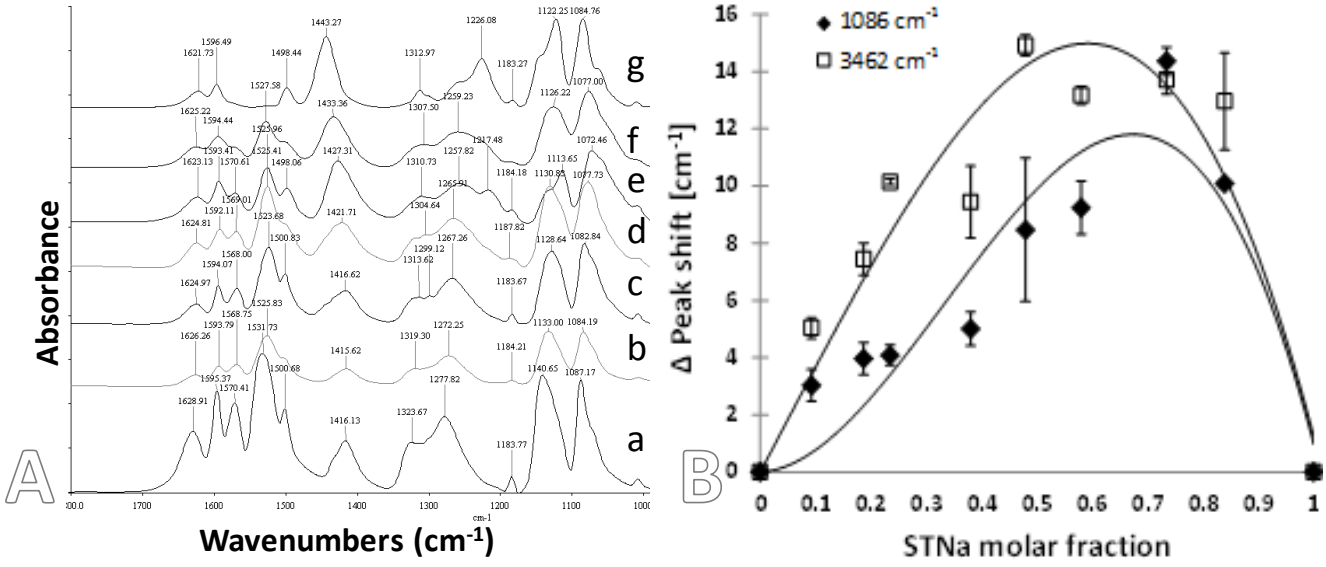

Figure 5A: FTIR spectrum in the 1800-1000 cm^{-1} range of a) spray dried ST; b) to f) spray dried ST:STNa in the ratios 9:1, 3:1, 1:3, 15:85 and g) FTIR spectrum of spray dried STNa. 5B: Job plot representation

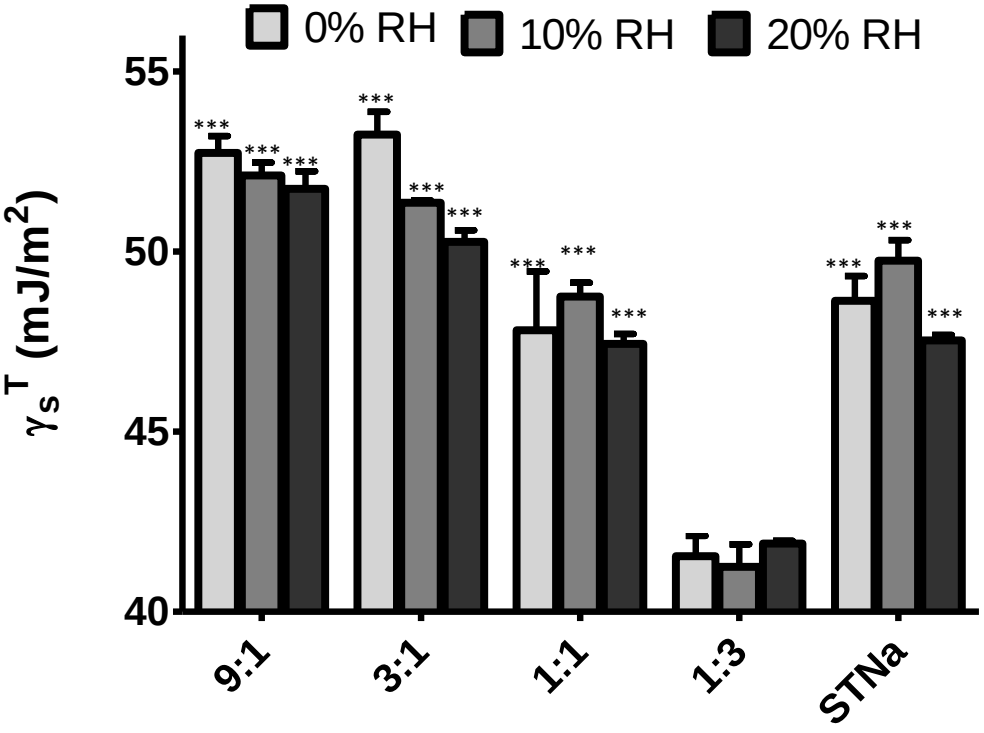

Figure 6: Total surface free energy for the different weight ratios (ST:STNa) at different %RH. Statistical analysis compares data obtained at the same RH value. System ST 1:3 was taken as reference of comparison for statistical post-hoc analysis. *** P<0.001

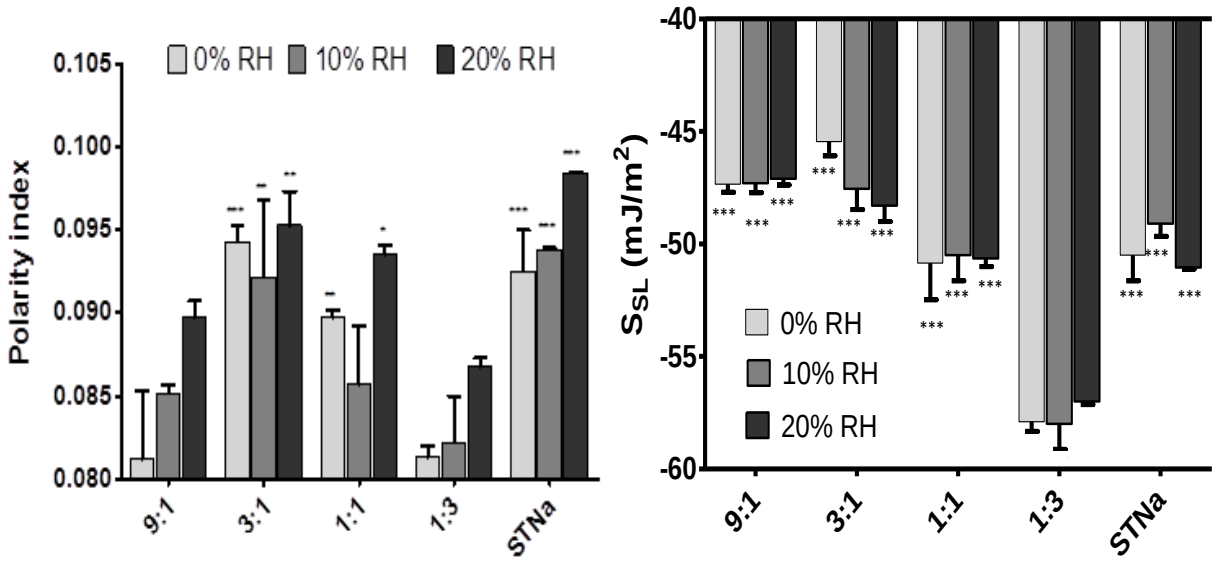

Figure 7: Polarity index (A) and spreading coefficient (B) changes for different weight ratios and %RH. Statistical analysis compares data obtained at the same RH value. System ST 1:3 was taken as reference of comparison for statistical post-hoc analysis *** P<0.001, ** P<0.01, * P < 0.05.

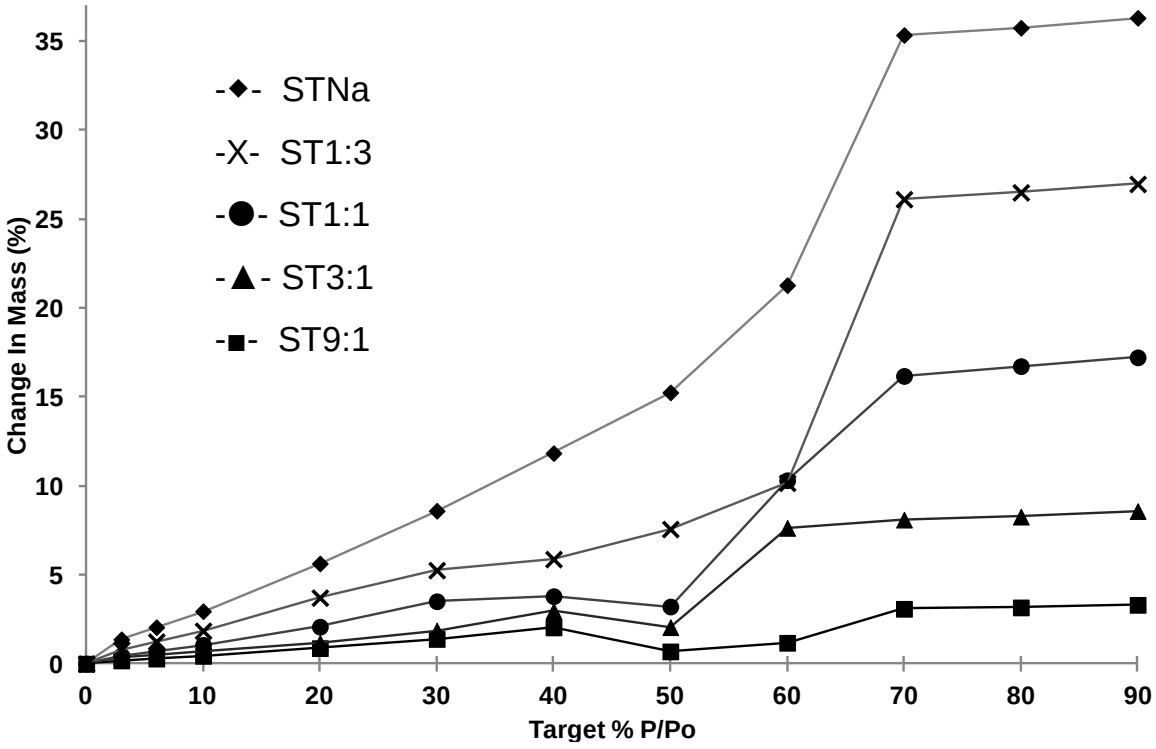

Figure 8: Water sorption isotherms for spray dried systems with different ST:STNa weight ratios.

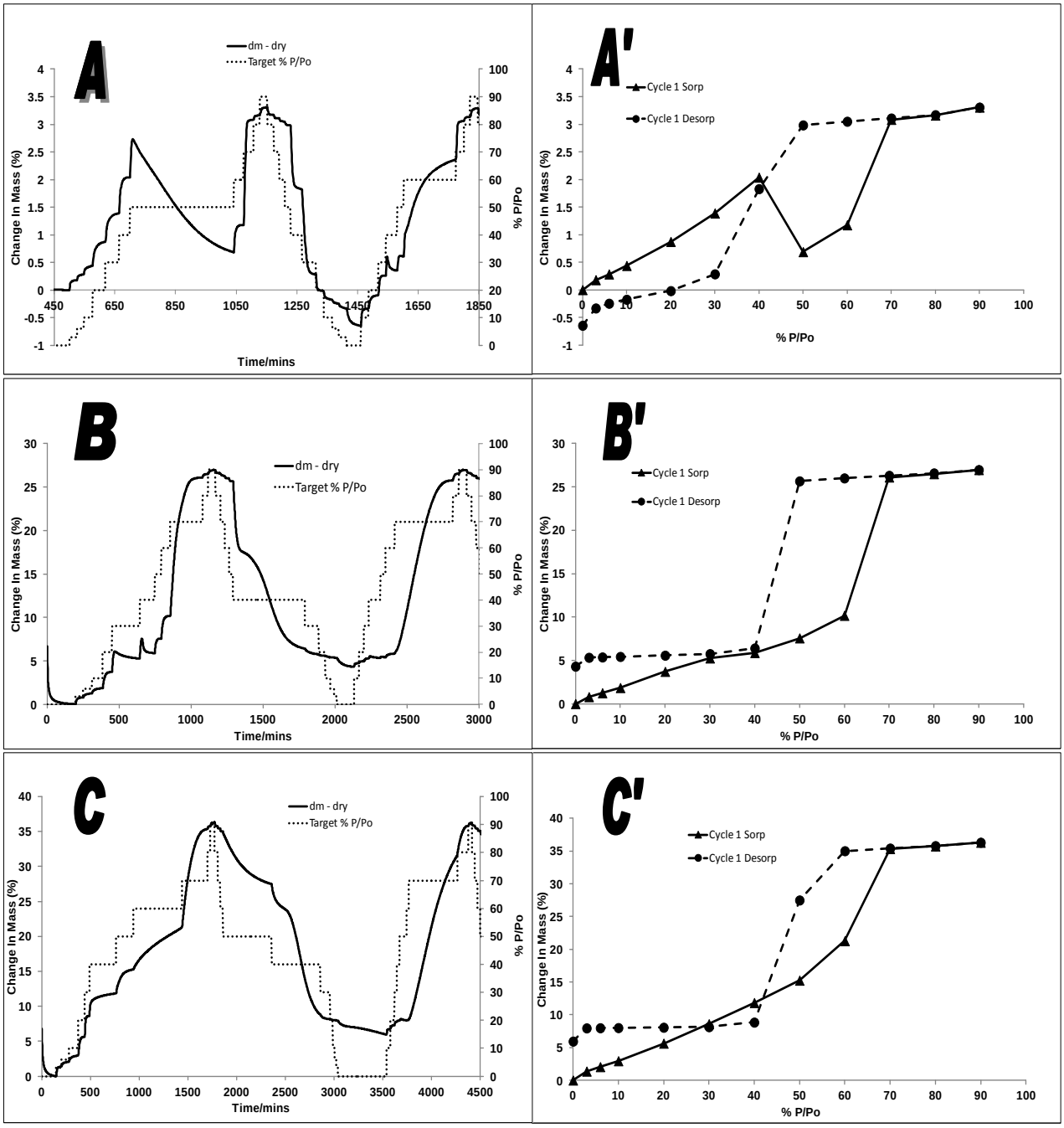

Figure 9 DVS kinetics (A, B, C) and isotherms (A', B', C') of: A-A') spray dried ST 9:1; B-B') spray dried ST 1:3; C-C') spray dried STNa.

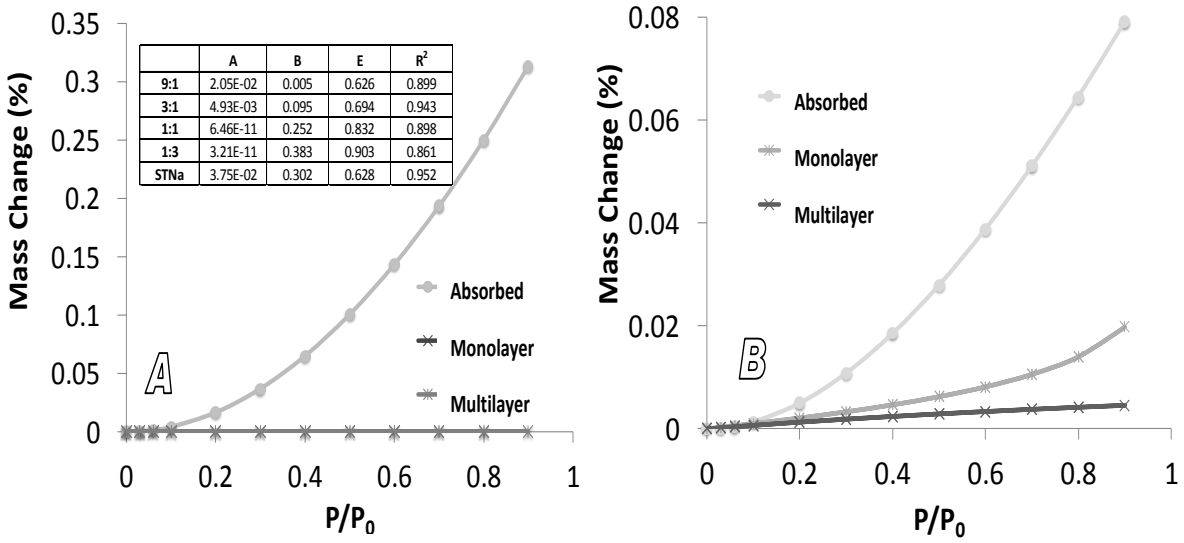

	A	B	E	R^2
9:1	2.05E-02	0.005	0.626	0.899
3:1	4.93E-03	0.095	0.694	0.943
1:1	6.46E-11	0.252	0.832	0.898
1:3	3.21E-11	0.383	0.903	0.861
STNa	3.75E-02	0.302	0.628	0.952

Figure 10: Moisture distribution patterns for 1:3 (A) and 3:1 (B) samples obtained by fitting experimental DVS results with the Young and Nelson equations. Estimated A, B, E Young and Nelson parameters and fit correlation coefficient for all the composites investigated are inserted in the chart (A).